Applied Physics A (2023) 129:302
https://doi.org/10.1007/s00339-023-06485-5

Applied Physics A
Materials Science & Processing

Analysis of friction and wear performance of Y_2O_3-doped Si_3N_4 ceramic using the estimation of stress

Qiang Wang[1] · Cunlong Zhou[1,2] · Chao Yang[1] · RuiJie Hao[1] · Yuanqing Yang[1]

Received: 19 November 2022 / Accepted: 10 February 2023 / Published online: 30 March 2023

Abstract
A variety of combinations of Y_2O_3 and Al_2O_3 were used as sintering aids in the fabrication of Si_3N_4 ceramics via gas pressure sintering (GPS). Based on the prediction of the residual thermal stress at the interface, the influence of crystal phases on the wear properties of Si_3N_4 ceramics was analyzed. As a result, with the increase of Y_2O_3 addition from 1 to 9 wt%, there are four kinds of crystal phases being firmly discovered in the sample, $Y_2Si_2O_7$, $YSiO_2N$, $Y_4Si_2O_7N_2$, and $Y_2Si_3O_3N_4$. The crystal phases of $Y_2Si_2O_7$, $YSiO_2N$, and $Y_4Si_2O_7N_2$ inhibit the particle flaking during the friction process, which greatly inhibited the progress of the abrasive wear, and optimize the wear resistance of silicon nitride ceramics. According to Selsing's model, it can be predicted that the interface residual thermal stress caused by the intergranular phase $Y_2Si_3O_3N_4$ is 22–35% higher than that caused by the other three intergranular phases. The crystal phase $Y_2Si_3O_3N_4$ intensifies the shedding of grains during wear, and reduces the wear performance of silicon nitride ceramics. In addition, the silicon nitride ceramics with 5wt% Y_2O_3 show better wear resistance, and the wear rate is 1.8×10^{-6} mm^3 N^{-1} m^{-1}.

Keywords Silicon nitride · Crystal phases · Residual thermal stress · Wear properties

1 Introduction

Si_3N_4 is an all-purpose ceramic with desirable mechanical properties, including excellent strength and low creep at high temperatures, thermal shock resistance, wear resistance, corrosion resistance, and appreciable theoretical thermal conductivities, which is ideal material for the preparation of wear-resistant basic parts [1–3]. At the same time, wear becomes the main reason for the failure of these components. Substantial efforts have been made to improve the wear resistance of silicon nitride ceramics [4–7]. Previous research has indicated that the wear properties of silicon nitride ceramic are greatly affected by the hardness ratio between the abrasive particles and the material matrix, and the specific wear rate is maximum when the abrasive particles are harder than the matrix [8]. Since the β-Si_3N_4 particles (20 Gpa) that exfoliated during the wear process are much harder than the Si_3N_4 (16–17 Gpa) ceramic matrix, the effective ways to improve the wear properties of silicon nitride ceramics are controlling the interfacial debonding. Francisco found that the existence of residual thermal stress at the interface promoted interface debonding [9]. Xue et al. [10] found that the residual thermal stress originating from the thermal expansion coefficient mismatches between the β-Si_3N_4 and the crystal phase.

Y_2O_3 is the most frequently used sintering aid in investigating and exploring the mechanical properties of silicon nitride. Quaternary Y–Si–O–N compounds are the frequently detected crystal phase in investigating Si_3N_4 ceramic when Y_2O_3 is used as sintering additive. It has been reported that there are six quaternary crystal phase being firmly discovered in the Y–Si–O–N family: Y_2SiO_5, $Y_2Si_2O_7$, $Y_5Si_3O_{12}N$, $YSiO_2N$, $Y_4Si_4O_7N_2$, and $Y_2Si_3O_3N_4$ [11, 12]. Moreover, the thermal expansion coefficients of these crystalline phases are obviously different [13–15].

However, to the authors' knowledge, little information is available on the relationship between the wear properties of silicon nitride ceramics and Y_2O_3. Therefore, the present study explores the wear performance of silicon nitride doped with Y_2O_3, focusing on the influence of crystal phase on

✉ Cunlong Zhou
1986048@tyust.edu.cn

[1] College of Mechanical Engineering, Taiyuan University of Science and Technology, Taiyuan 030024, China

[2] Shan Xi Provincial Key Laboratory of Metallurgical Device Design Theory and Technology, Taiyuan University of Science and Technology, Taiyuan 030024, China

wear performance of silicon nitride ceramics. This study provides technical guidance for optimizing the preparation process of Si3N4 ceramic.

2 Estimation model of interface residual thermal stress

2.1 Generation of interface residual thermal stress

Figure 1 shows the transformation process of the α phase to the β phase in Si_3N_4. SiO_2 is an inevitable phase in Si_3N_4 powders. The sintering aid reacted with the SiO_2 film on the surface of the Si_3N_4 powder in an oxidation–reduction manner, thereby removing SiO_2 and generating a liquid phase. α-Si_3N_4 dissolves in the liquid phase generated by the sintering aid, and when the solution reaches saturation, it precipitated out again as β-Si_3N_4 and existed in the form of rod-like β-Si_3N_4 after cooling. In this process, the residual thermal stress caused by thermal expansion mismatch between crystal phase and β-Si_3N_4 may promote interface debonding of Si_3N_4 ceramics.

2.2 Thermal expansion coefficient of crystal phase

The thermal expansion coefficient of each crystal phase in the SiO_2–Y_2O_3–Si_3N_4 system was calculated using the bond valence model. For a multicomponent compound system with n types of binary systems, its thermal expansion coefficient can be obtained on the basis of the definition by the following equation [16]:

$$\alpha = \sum_{\mu=1}^{n} v_l^{\mu} \alpha_l^{\mu}, \tag{1}$$

v_l^{μ} and α_l^{μ} can be calculated as

$$v_l^{\mu} = \frac{\left(n^{\mu} R_{ij,\mu}^3\right)^{1/3}}{\sum_{\mu=1}^{n} \left(n^{\mu} R_{ij,\mu}^3\right)^{1/3}} \tag{2}$$

$$\alpha_l^{\mu} = \frac{1.35 k R_{ij}}{\gamma \left(\frac{8 S_{ij}}{3}\right)^{3/2} \left(\frac{1}{b} - \frac{2}{R_{ij}}\right)} \tag{3}$$

$$S_{ij} = \left(\frac{R_0 - R_{ij}}{b}\right), \tag{4}$$

where a is the linear thermal expansion coefficient of the intergranular phase, $\gamma = 23\text{nN}\text{Å}^2$ (electrons)$^{-2}$, R_{ij} is the length of the bond between the two atoms i and j, b is a universal constant equal to 0.37 Å, R_0 is the bond valence parameter, k is the Boltzmann constant, μ represents the bond type in the unit cell, and n represents the number of binary systems in the unit cell. The binary structural units,

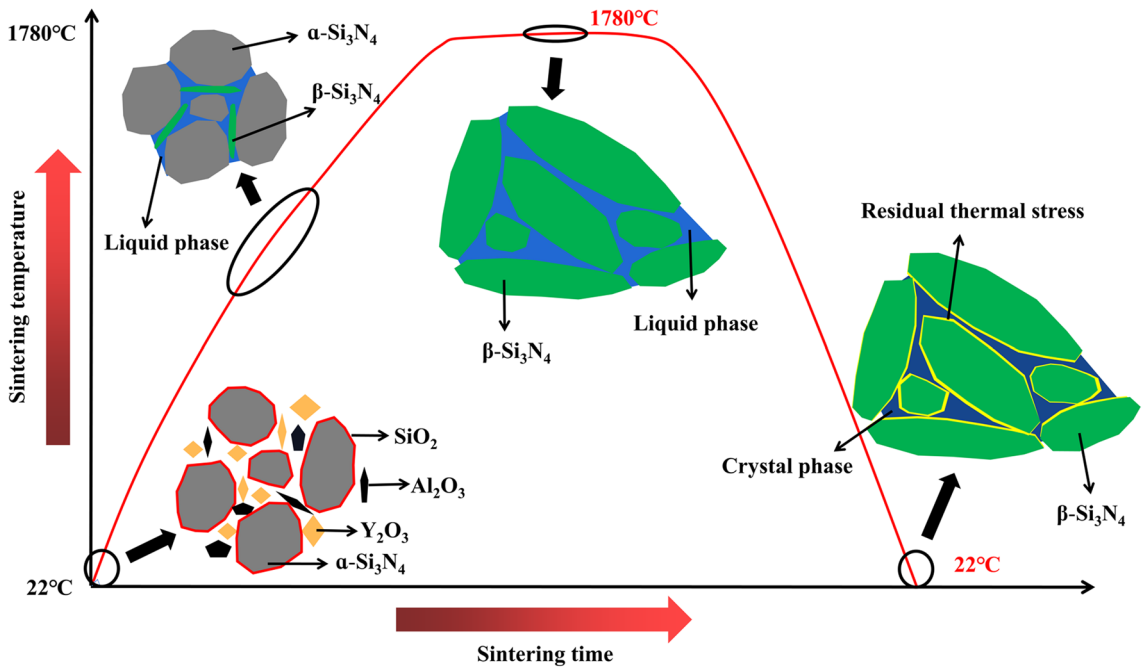

Fig. 1 Schematic diagram of α → β phase transition in silicon nitride sample

Table 1 Structural units, calculated average bond lengths (Å), and bond valence parameter (R_0) of $Y(O/N)_n$ polyhedra and $Si(O/N)_4$ tetrahedra of the six Y–Si–O–N quaternary compounds [14, 17]

Compounds	Structural units		Average bond length (Å)		R_0
			$Y(O/N)_n$	$Si(O/N)_4$	
$Y_2Si_2O_7$	$Y–O_6$	$Si–O_4$ $O_1–Si_2$	2.028	1.624	0.37
Y_2SiO_5	$Y_1–O_7$ $Y_2–O_6$ $O_1–Y_4$	$Si–O_4$ $O_2–SiY_3$	2.019	1.622	0.37
$Y_5Si_3O_{12}N$	$Y_1–O_8N$ $Y_2–O_7$ $Y_3–O_6N$ $Y_4–O_7$	$Si_1–O_4$ $Si_2–O_4$ $Si_3–O_3N$	2.378	1.612	0.37
$YSiO_2N$	$Y_1–O_6N_2$ $Y_2–O_6N_2$ $Y_3–O_6N_2$	$Si_1–O_2N_2$ $Si_2–O_2N_2$	2.438	1.648	0.37
$Y_4Si_2O_7N_2$	$Y_1–O_5N_2$ $Y_2–O_7$ $Y_3–O_5N$ $Y_4–O_5N_2$	$Si_1–O_2N_2$ $Si_2–O_3N$	2.331	1.643	0.37
$Y_2Si_3O_3N_4$	$Y_1–O_3N_5$ $Y_2–O_5N_3$	$Si_1–ON_3$ $Si_2–ON_3$ $Si_3–O_2N_2$	2.478	1.671	0.37

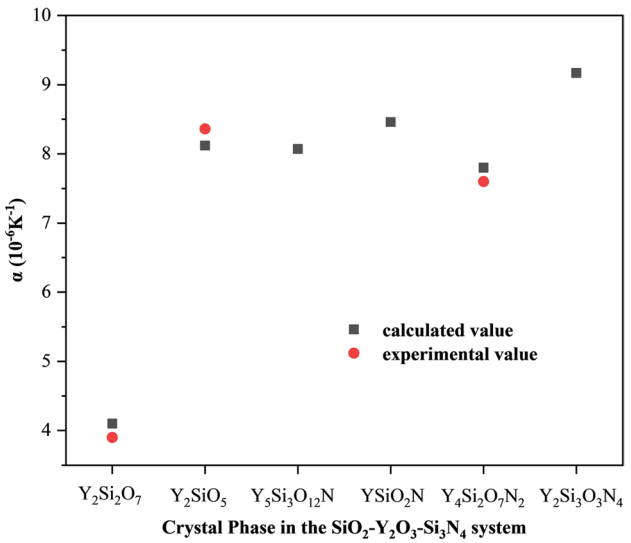

Fig. 2 Thermal expansion coefficient of crystal phase

bond length, and bond valence parameters of the six crystal phases are shown in Table 1.

Figure 2 shows the calculated and experimental values of the thermal expansion coefficients of the six crystal phases of the SiO_2–Y_2O_3–Si_3N_4 system. The experimental values were obtained from literatures [13–15]. Here, all the experimental thermal expansion coefficients are those at or near room temperature in the available literatures. Wherein, the calculated thermal expansion coefficients of crystal phases Y_2SiO_5, $Y_2Si_2O_7$, $Y_5Si_3O_{12}N$, $YSiO_2N$, $Y_4Si_2O_7N_2$, and $Y_2Si_3O_3N_4$ are 4.1×10^{-6} K^{-1}, 8.1×10^{-6} K^{-1}, 8.07×10^{-6} K^{-1}, 8.46×10^{-6} K^{-1}, 7.8×10^{-6} K^{-1}, and 9.17×10^{-6} K^{-1}, respectively. The calculated values of thermal expansion coefficient were compared with the experimental data, and the good agreement demonstrates the predictive power of Eq. (1).

2.3 Residual thermal stresses

According to Selsing's model [18, 19], the interfacial thermal residual stress between the crystal phase and silicon nitride could be calculated by

$$\sigma_r = \frac{\Delta\alpha \cdot \Delta T}{\frac{1-2\nu_1}{E_1} + \frac{(1+\nu_2)}{2E_2}}, \tag{5}$$

where,σ_r, $\Delta\alpha$, ΔT, ν, and E are the interfacial thermal residual stress, difference in coefficient of thermal expansion (CTE), temperature range over which stress is not relieved, Poisson's ratio, and elastic modulus, respectively. The subscripts 1 and 2 refer to the crystal phase and silicon nitride, respectively. The physical properties of the β-Si3N4 and the crystal phase are shown in Table 2.

Figure 3 shows the residual thermal stress at the interface between crystal phase and β-Si_3N_4. The residual thermal stress around crystal phases of Y_2SiO_5, $Y_2Si_2O_7$, $Y_5Si_3O_{12}N$, $YSiO_2N$, $Y_4Si_2O_7N_2$, and $Y_2Si_3O_3N_4$ are 37.53 MPa, 453.23 MPa, 524.44 MPa, 529.25 MPa, 442.64 MPa, and 678.4 MPa, respectively. The residual thermal stress of the samples with introducing crystal phases of $Y_2Si_2O_7$, $Y_4Si_2O_7N_2$, Y_2SiO_5, $Y_5Si_3O_{12}N$, and $YSiO_2N$ shows a continuous upward trend. At the same time, the generation of the crystal phase $Y_2Si_3O_3N_4$

Table 2 Physical properties of β-Si_3N_4, Y_2SiO_5, $Y_2Si_2O_7$, $Y_5Si_3O_{12}N$, $YSiO_2N$, $Y_4Si_2O_7N_2$, and $Y_2Si_3O_3N_4$

Compounds	Young's modulus (E, GPa)	Poisson's ratio (ν)	Thermal expansion (α, K^{-1})
β-Si_3N_4	300[20]	0.28 [21]	3.5×10^{-6} [21]
$Y_2Si_2O_7$	155 [14, 15]	0.27 [14]	4.1×10^{-6}
Y_2SiO_5	124 [14, 15]	0.31 [14]	8.1×10^{-6}
$Y_5Si_3O_{12}N$	204 [22]	0.29 [22]	8.07×10^{-6}
$YSiO_2N$	196 [22]	0.27 [22]	8.46×10^{-6}
$Y_4Si_2O_7N_2$	191 [15, 22]	0.28 [22]	7.8×10^{-6}
$Y_2Si_3O_3N_4$	244 [22]	0.27 [22]	9.17×10^{-6}

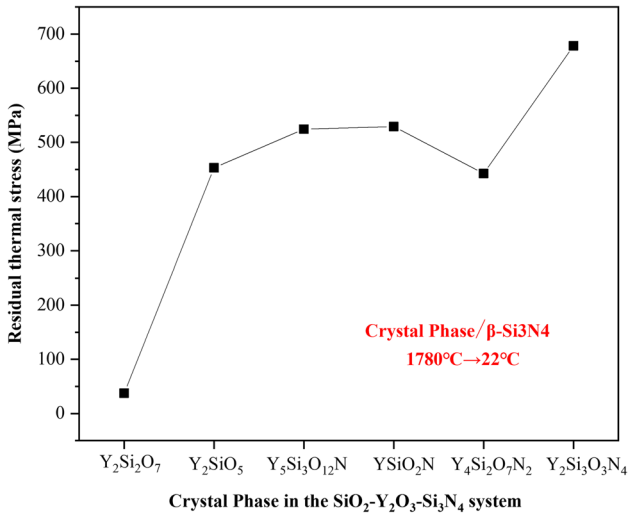

Fig. 3 Residual thermal stress between the crystal phase and silicon nitride

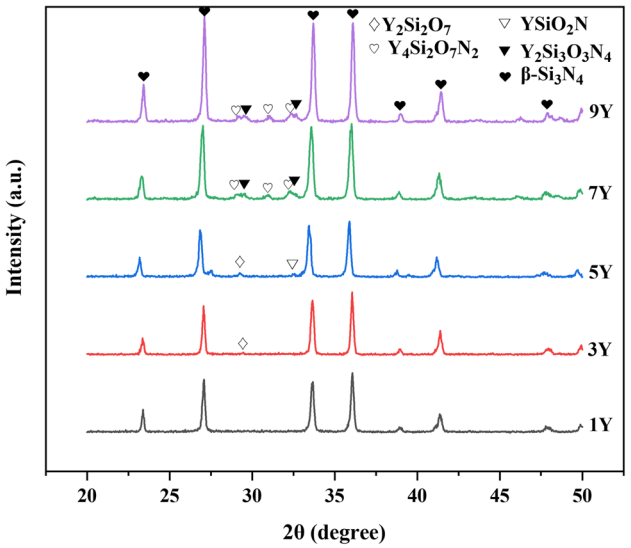

Fig. 4 XRD results of Si_3N_4 samples

significantly increases the residual thermal stress at the interface, which may aggravate interface peeling during the wear process and reduce the wear performance of silicon nitride ceramic.

3 Materials and methods

3.1 Raw materials and experimental procedure

Si_3N_4, (E10 α-Si3N4, UBE, Japan), Y_2O_3, and Al_2O_3 powders (Shanghai Naiou Nanotechnology Co., Ltd.) were used as raw materials in this study. The raw materials were mixed according to the ratios given in Table 3.

The α-Si_3N_4 powder was mixed with Y_2O_3 and Al_2O_3 with agate balls in a nylon jar for 12 h in a planetary mill, using ethanol as a mixing medium. The slurries were dried at 80 °C. The mixed powder was milled and sieved through 80-screen sieve. After being uniaxially dry pressed at 50 MPa and cold isostatically pressed at 230 MPa, the green samples were sintered at 1780 °C under 100 bar nitrogen pressure, followed by furnace cooling down to room temperature (22 °C).

Table 3 The composition for each sample

Designation	Si_3N_4 (wt%)	Y_2O_3 (wt%)	Al_2O_3 (wt%)	Sintering method	Temperature (℃)
1Y	94	1	5	Gas pressure sintering	1780
3Y	92	3	5		
5Y	90	5	5		
7Y	88	7	5		
9Y	86	9	5		

3.2 Characterization

An X-ray diffractometer was used to characterize the phase structure of sintered samples. The step size was set at 0.03° in a diffraction angle range of 20°–50°, and the scanning rate of 1°/min.

The wear properties of the samples were tested using the Rtec multifunctional friction and wear tester (MFT-5000, USA). Polished commercial Si_3N_4 balls (Sinoma High-tech Nitride Ceramics Co., Ltd.) with a diameter of 5.56 mm were used as friction pairs. At room temperature (22 ℃), the friction pairs moves is a reciprocating relative motion. The load, stroke, and frequency of reciprocation were all set to 40 N, 4 mm, and 3 Hz, respectively.

After the wear test, the worn surface morphology of the sample was observed using scanning electron microscopy (SEM).

Meanwhile, the depth of the worn surface was measured using laser confocal microscopy.

Finally, a VHX6000 ultradepth-of-field 3D contour graph (Keyence Corporation, Japan) was used to measure the topography profile curves of worn after the test. Then, using the formula $k=A/2(P\times f\times t)$ to calculate wear rates. A is the area of topography profile of worn surface which determined by ultradepth-of-field 3D contour graph, P is the applied load, f is sliding frequency, and t is total sliding time.

4 Results and discussion

4.1 Phase composition

Figure 4 shows the XRD patterns obtained for the as-sintered samples with different Y_2O_3 content. It can be seen that all main peaks are characteristic β-Si_3N_4 peaks, which indicates that the α-phase has been completely transformed into the β phase during the sintering. For Y_2O_3 content of 1 wt%, no other peaks were observed except for the characteristic β-Si3N4 peaks. For the sample with 3 wt% Y_2O_3, in addition to the β-phase peaks, low-intensity peaks characteristic for $Y_2Si_2O_7$ were detected. In the samples with 5 wt% Y_2O_3, the $Y_2Si_2O_7$ and $YSiO_2N$ phase was found. For Y_2O_3 content of 7 and 9 wt%, the $Y_4Si_2O_7N_2$ phase was found.

The chemical reactions for the formation of the $Y_2Si_2O_7$, $YSiO_2N$, $Y_4Si_2O_7N_2$, and $Y_2Si_3O_3N_4$ phases are as follows [23–26]:

$$Y_2O_3 + 2SiO_2 \rightarrow Y_2Si_2O_7 \quad (6)$$

$$2Y_2O_3 + SiO_2 + Si_3N_4 \rightarrow 4YSiO_2N \quad (7)$$

$$4Y_2O_3 + SiO_2 + Si_3N_4 \rightarrow 2Y_4Si_2O_7N_2 \quad (8)$$

$$Y_2O_3 + Si_3N_4 \rightarrow Y_2Si_3O_3N_4. \quad (9)$$

It can also be seen from the above that when the ratio of Y_2O_3/SiO_2 is 1/2, 2/1, 4/1, and 1/0, the corresponding crystal phases are $Y_2Si_2O_7$, $YSiO_2N$, $Y_4Si_2O_7N_2$, and $Y_2Si_3O_3N_4$, respectively.

4.2 Wear behavior

Figure 5 shows the wear surface morphologies of the samples. When the Y_2O_3 content was 1%, recurrent loads induced surface fatigue and crack, as shown in Fig. 5a. As the wear progressed, the cracks propagated and the scale debris accumulation layer were exfoliated, and then, a new surface was exposed. The surface morphology of the Si_3N_4 ceramics with 3wt% and 5wt% Y_2O_3 after Wear test is shown in Fig. 5b, c, respectively. The wear debris adhered to each other during the wear process. Most area of the surface remains smooth, and surface fatigue and crack occurred in a few isolated areas. When the Y_2O_3 content increased to 7%, wear took away the debris accumulation layer to expose a new surface, and Si_3N_4 particles' exfoliation resulted in the wear intensified, as shown in Fig. 5d. When the Y_2O_3 content increased to 9%, accompanied by large debris accumulation layer removed, the wear surface

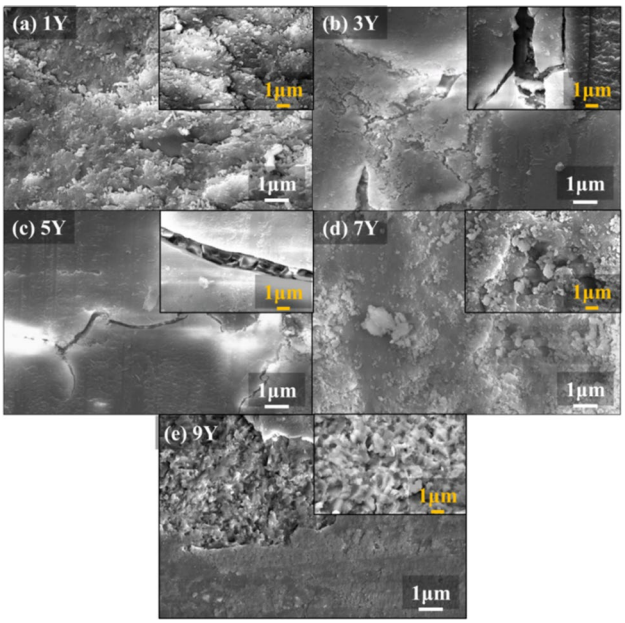

Fig. 5 Scanning electron micrographs (SEM) of the wear surface morphologies on the Si3N4 tested at 22 ℃ under a load of 40 N

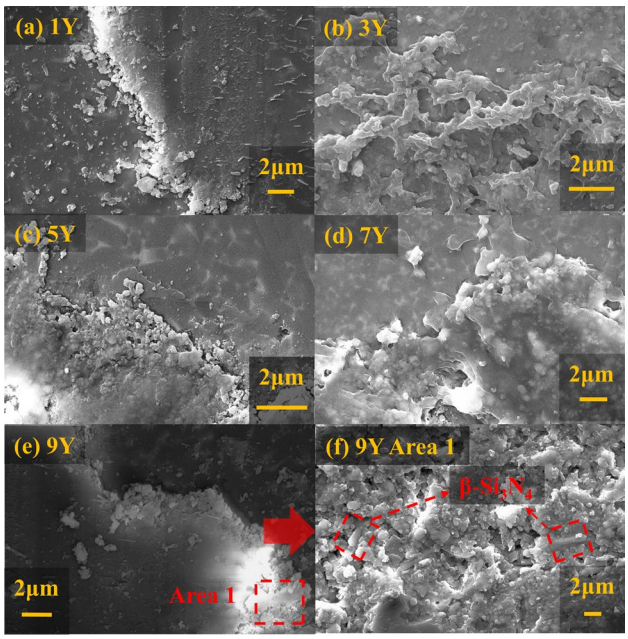

Fig. 6 Wear debris morphology of wear surface

has the appearance of a typical fracture surface of silicon nitride, indicating a possible intergranular fracture, as shown in Fig. 5e. This observation suggests that interface peeling is the predominant mode of wear.

To analyze wear mechanism of Si_3N_4 ceramics by adding Y_2O_3, the debris morphology of wear surface was also observed and analyzed. The morphology of the wear debris

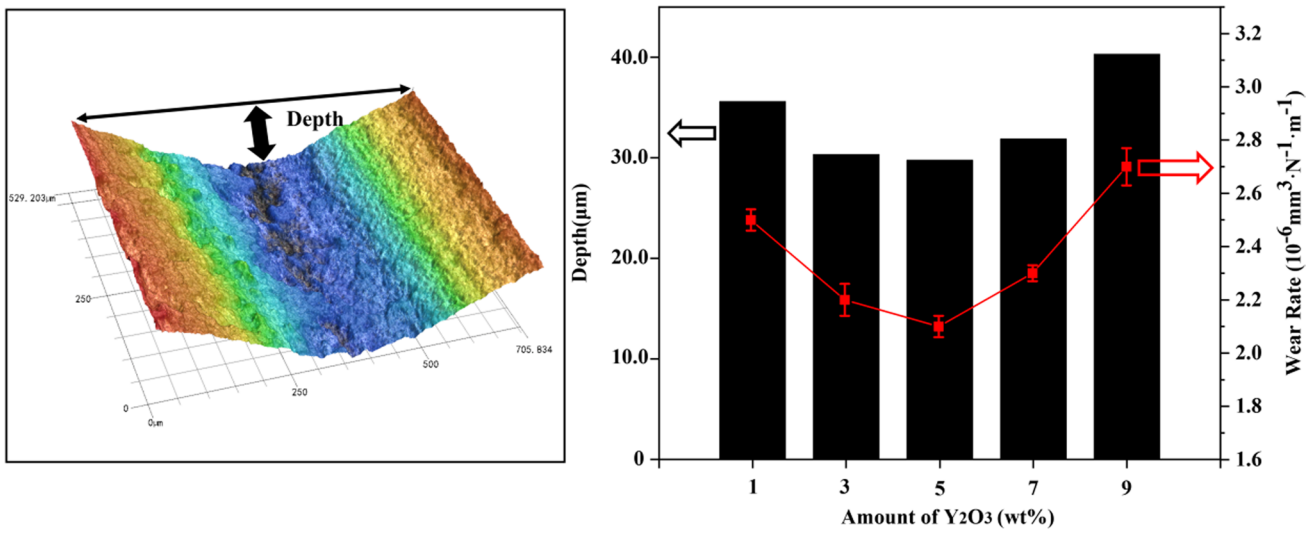

Fig. 7 Cross-sectional depth of the Si_3N_4 ceramic sample wear track and wear rate

of the Si_3N_4 ceramic with 1, 3, and 5 wt% Y_2O_3 is block-like debris, as shown in Fig. 6a–c. This showed that surface fatigue is the dominant wear mechanism in Si_3N_4 ceramics. For the Si_3N_4 ceramic with 7 and 9 wt% Y_2O_3, the morphology of the wear debris is particle-like debris and β-Si_3N_4, as shown in Fig. 6d–f. This showed that abrasive wear is the dominant wear mechanism in Si_3N_4 ceramics. Based on the above analysis, the existence of $Y_2Si_3O_3N_4$ phases caused a large residual thermal stress at the interface, and thus increased the β-Si_3N_4 fracture of subsurface during the wear process, which greatly promoted the progress of abrasive wear.

4.2.1 Wear surface depth and wear rate

The wear depth and the wear rate of the silicon nitride ceramics are shown in Fig. 7. When the Y_2O_3 content increased from 1 to 5%, the wear depth decreased from 35.6 μm to 29.8 μm, and the wear rate of the silicon nitride ceramics decreased from 2.5×10^{-6} mm^3 to 1.8×10^{-6} mm^3 N^{-1} m^{-1}. The wear depth and wear rate increased by 35.2% and 53.8% after the Y_2O_3 content increased from 5 wt% to 9 wt%. Obviously, the silicon nitride ceramics with 5wt% Y_2O_3 shows better wear resistance. Since the less residual thermal stress is helpful to improved the fracture toughness of the silicon nitride ceramics [27], thereby inhibiting particle flaking during the friction process. As discussed in Sects. 2.3 and 4.2, the crystal phases of $Y_2Si_2O_7$, $YSiO_2N$, and $Y_4Si_2O_7N_2$ inhibit the particle flaking during the friction process, which greatly inhibited the progress of the abrasive wear and optimize the wear resistance of silicon nitride ceramics. However, the residual thermal stress at the interface caused by the crystal phase $Y_2Si_3O_3N_4$ was 22–35% higher than that caused by the above three crystal phases. The interface between crystal phase $Y_2Si_3O_3N_4$ and Si3N4 matrix would be debonded due to the excessive residual thermal stress, intensifies the shedding of grains during wear, and reduces the wear performance of silicon nitride ceramics.

5 Conclusions

A variety of combinations of Y_2O_3 and Al_2O_3 were used as sintering aids in the fabrication of Si_3N_4 ceramics via gas pressure sintering (GPS). Based on the prediction of the residual thermal stress at the interface, the influence of crystal phases on the wear properties of Si_3N_4 ceramics was analyzed. The following conclusions were drawn:

1. The crystal phases, $Y_2Si_2O_7$, $YSiO_2N$, $Y_4Si_2O_7N_2$, and $Y_2Si_3O_3N_4$, were formed in silicon nitride ceramics during sintering. The interface residual thermal stress caused by the crystal phase $Y_2Si_3O_3N_4$ is 22–35% higher than that caused by the other three crystal phases.
2. The crystal phases of $Y_2Si_2O_7$, $YSiO_2N$, and $Y_4Si_2O_7N_2$ inhibit the particle flaking during the friction process, which greatly inhibit the progress of the abrasive wear and optimize the wear resistance of silicon nitride ceramics.
3. The interface between crystal phase $Y_2Si_3O_3N_4$ and Si_3N_4 matrix would be debonded due to the exces-

sive residual thermal stress, intensifies the shedding of grains during wear, and reduces the wear performance of silicon nitride ceramics.

Acknowledgements This work was supported by Science and Technology Major Project of Shanxi Province, China (20181102015), and Science and Technology Project of Taiyuan, Unveiled Project of Taiyuan.

Author contributions QW and CZ: wrote the main manuscript text; CY: analyzed the data; RH and YY: experiment.

Data and code availability The raw/processed data required to reproduce these findings cannot be shared at this time as the data also form part of an ongoing study.

Declarations

Conflict of interest There is no conflict of interest with others.

Ethics approval No human tissue or animal subjects were involved in this study.

References

1. L. Wang, R.W. Snidle, L. Gu, Rolling contact silicon nitride bearing technology: a review of recent research. Wear **246**, 159–173 (2000)
2. F. Caretto, A.M. Laera, F. Di Nuzzo, R. Iovino, F. Di Benedetto, E. Pesce, M. Re, M. Schwarz, L. Tapfer, Molybdenum disilicide-silicon nitride bushing nozzles tailor-made for basalt fifibers production. Ceram. Int. **42**, 11844–11850 (2016)
3. R. Danzer, M. Lengauera, W. Zleppnig, W. Harrer, Silicon nitride tools for hot rolling of high-alloyed steel and superalloy wire-load analysis and first practical tests. Int. J. Mat. Res. **98**, 1104–1114 (2007)
4. F. Brenscheidt, S. Oswald, A. Miicklich, E. Wieser, W. Mijller, Wear mechanisms in titanium implanted silicon nitride ceramics. Nucl. Inst. Methods Phys. Res. B **129**, 483–486 (1997)
5. J. Kang, M. Hadfield, The influence of heterogeneous porosity on silicon nitride/steel wear in lubricated rolling contact. Ceram. Int. **26**, 315–324 (2000)
6. A. Kumar, S. Ghosh, Aravindan, Grinding performance improvement of silicon nitride ceramics by utilizing nanoflfluids. Ceram. Int. **43**, 13411–13421 (2017)
7. Q. Tang, J. Chen, L. Liu, Tribological behaviours of carbon fifibre reinforced PEEK sliding on silicon nitride lubricated with water. Wear **269**, 541–546 (2010)
8. L. Wang, Z. Qiao, Q. Qi, Y. Yu, T. Li, X. Liu, Z. Huang, H. Tang, W. Liu, Improving abrasive wear resistance of Si3N4 ceramics with self-matching through tungsten induced tribochemical wear. Wear **494–495**, 204254 (2022)
9. S. Funfschilling, T. Fett, M.J. Hoffmann, Mechanisms of toughening in silicon nitrides: The roles of crack bridging and microstructure. Acta Mater. **59**, 3978–3989 (2011)
10. W. Xue, J. Yi, Z. Xie, W. Liua, J. Chen, Enhanced fracture toughness of silicon nitride ceramics at cryogenic temperatures. Scripta Mater. **66**, 891–894 (2012)
11. I.K. Naik, L.J. Gauckler, T.Y. Tien, Solid-liquid equilibria in the system Si_3N_4-AIN-SiO_2-Al_2O_3. J. Am. Ceram. Soc. **61**, 332–335 (1978)
12. Y.-N. Xu, P. Rulis, W.Y. Ching, Electronic structure and bonding in quaternary crystal $Y_3Si_5N_9O$. Phys. Rev. B. **72**, 1–4 (2005)
13. Z. Sun, Y. Zhou, J. Wang, M. Li, Thermal Properties and Thermal Shock Resistance of c-$Y_2Si_2O_7$. J. Am. Ceram. Soc. **91**, 2623–2629 (2008)
14. Z. Sun, J. Wang, M. Li, Y. Zhou, Mechanical properties and damage tolerance of Y_2SiO_5. J. Eur. Ceram. Soc. **28**, 2895–2901 (2008)
15. L. Sun, B. Liu, J. Wang, J. Wang, Y. Zhou, Hu. Zijun, $Y_4Si_2O_7N_2$: a new oxynitride with low thermal conductivity. J. Am. Ceram. Soc. **95**, 3278–3284 (2012)
16. X. Liu, H. Wang, W. Wan, Fu. Zhengyi, A prediction model of thermal expansion coeffificient for cubic inorganic crystals by the bond valence model. J. Solid State Chem. **299**, 1–13 (2021)
17. L. Sun, B. Liu, J. Wang, Z. Li, J. Wang, Theoretical study on the relationship between crystal chemistry and properties of quaternary Y-Si-O-N oxynitrides. J. Am. Ceram. Soc. **99**, 2442–2450 (2016)
18. R. Wang, W. Li, D. Li, D. Fang, New temperature dependent fracture strength model for the ZrB2-SiC composites. J. Eur. Ceram. Soc. **35**, 2957–2962 (2015)
19. J. Selsing, Internal stresses in ceramics. J. Am. Ceram. Soci. **44**, 419 (1961)
20. I.M. Peterson, T.-Y. Tien, Effect of the grain boundary thermal expansion coefficient on the fracture toughness in silicon nitride. J Am. Cwam Sac. **78**, 2345–2352 (1995)
21. R. van Weeren, S.C. Danforth, The effect of grain boundary phase characteristics on the crack deflection biehavior in asilicon nitride material. Scripta Mater. **34**, 1567–1573 (1996)
22. Y. Zhou, H. Hyuga, D. Kusano, C. Matsunaga, K. Hirao, Effects of yttria and magnesia on densification and thermal conductivity of sintered reaction-bonded silicon nitrides. J. Am. Ceram. Soc. **102**, 1579–1588 (2019)
23. M. Kitayama, Thermal Conductivity of β-Si_3N_4: Effect of Lattice Oxygen. J. Am. Ceram. Soc. **83**, 1985–1992 (2000)
24. Z. Luo, W. Liu, Qu. Gao, Lu. Anxian, G. Han, Sintering behavior, microstructure and mechanical properties of various fluorine-containing Y-SiAlON glass-ceramics. J. Non-Cryst. Solids **388**, 62–67 (2014)
25. W. Liu, W. Tong, R. He, Wu. Haidong, Wu. Shanghua, Effect of the Y_2O_3 additive concentration on the properties of a silicon nitride ceramic substrate. Ceram. Int. **42**, 18641–18647 (2016)
26. W. Wang, D. Yaoa, H. Liang, Y. Xia, K. Zuo, J. Yin, Y.-P. Zeng, Effffect of in-situ formed Y_2O_3 by metal hydride reduction reaction on thermal conductivity of β-Si_3N_4 ceramics. J. Eur. Ceram. Soc. **40**, 5316–5323 (2020)
27. L.J. Wang, Q. Qi, X. Yang, Mechanical properties optimization of Si_3N_4 ceramics by in-situ introduction of core-shell structural W-Fe_5Si_3. Compos. B Eng. **196**, 1–9 (2020)